Investigating photoluminescence properties of Ca-doped ZnS nanoparticles prepared via hydrothermal method

Abdelghafour Said Messalti, Malika El-Ghozzi, Daniel Zambon, Rachid Mahiou, Zouaoui Setifi

▶ **To cite this version:**

Abdelghafour Said Messalti, Malika El-Ghozzi, Daniel Zambon, Rachid Mahiou, Zouaoui Setifi. Investigating photoluminescence properties of Ca-doped ZnS nanoparticles prepared via hydrothermal method. Journal of Luminescence, 2021, 238, 10.1016/j.jlumin.2021.118227 . hal-03445530

HAL Id: hal-03445530
https://hal.science/hal-03445530

Submitted on 24 Nov 2021

HAL is a multi-disciplinary open access archive for the deposit and dissemination of scientific research documents, whether they are published or not. The documents may come from teaching and research institutions in France or abroad, or from public or private research centers.

L'archive ouverte pluridisciplinaire **HAL**, est destinée au dépôt et à la diffusion de documents scientifiques de niveau recherche, publiés ou non, émanant des établissements d'enseignement et de recherche français ou étrangers, des laboratoires publics ou privés.

Journal Pre-proof

Investigating photoluminescence properties of Ca-doped ZnS nanoparticles prepared via hydrothermal method

Abdelghafour Said Messalti, Malika El-Ghozzi, Daniel Zambon, Rachid Mahiou, Zouaoui Setifi

PII: S0022-2313(21)00343-4

DOI: https://doi.org/10.1016/j.jlumin.2021.118227

Reference: LUMIN 118227

To appear in: *Journal of Luminescence*

Received Date: 26 October 2020

Revised Date: 28 April 2021

Accepted Date: 19 May 2021

Please cite this article as: A.S. Messalti, M. El-Ghozzi, D. Zambon, R. Mahiou, Z. Setifi, Investigating photoluminescence properties of Ca-doped ZnS nanoparticles prepared via hydrothermal method, *Journal of Luminescence*, https://doi.org/10.1016/j.jlumin.2021.118227.

This is a PDF file of an article that has undergone enhancements after acceptance, such as the addition of a cover page and metadata, and formatting for readability, but it is not yet the definitive version of record. This version will undergo additional copyediting, typesetting and review before it is published in its final form, but we are providing this version to give early visibility of the article. Please note that, during the production process, errors may be discovered which could affect the content, and all legal disclaimers that apply to the journal pertain.

© 2021 Published by Elsevier B.V.

Journal Pre-proof

CRediT authorship contribution statement

A.S. Messalti : Investigation, Data curation, Writing – original draft

M. El-Ghozzi : Data curation, Formal analysis, Visualization, Validation

D. Zambon : Supervision, Validation, Visualization, Project administration, Writing - review & editing

R. Mahiou : Data curation, Formal analysis, Visualization, Validation

Z. Setifi : Supervision, Validation, Visualization, Project administration, Funding acquisition.

Journal Pre-proof

Journal Pre-proof

Investigating photoluminescence properties of Ca-doped ZnS nanoparticles prepared via hydrothermal method

Abdelghafour Said Messalti [a,b,c*], Malika El-Ghozzi [c], Daniel Zambon [c*], Rachid Mahiou [c], Zouaoui Setifi [b]

[a] Département de Physique, Faculté des Sciences, Université Ferhat Abbas Sétif 1, Sétif 19000, Algeria.

[b] Laboratoire de Chimie, Ingénierie Moléculaire et Nanostructures (LCIMN), Université Ferhat Abbas Sétif 1, Sétif 19000, Algeria.

[c] Université Clermont Auvergne, Institut de Chimie de Clermont-Ferrand, UMR 6296 CNRS/UBP/Sigma Clermont, TSA 60026 CS 60026, F-63000 Clermont-Ferrand, France.

*E-mail address : daniel.zambon@uca.fr (corresponding author).

abdelghafour-messalti@hotmail.com (corresponding author)

Journal Pre-proof

Abstract

The structural, morphological and optical properties of pure and Ca-doped zinc sulfide (ZnS:Ca) nanoparticles (NPs) prepared by hydrothermal method at different percentages of Ca are reported herein. The resulting NPs were characterized by X-ray diffraction analysis (XRD), Raman scattering, scanning electron microscopy (SEM), transmission electron microscopy (TEM) and photoluminescence (PL) spectroscopy. The XRD patterns confirmed the crystalline nature of all pure and doped NPs showing a single phase cubic blende structure, whereas the

SEM micrographs showed sphere-shaped NPs. The sizes of the as-prepared NPs estimated by TEM were found to be in the range 44-147 nm. The PL emission spectra of ZnS:Ca nanocrystals excited at 400 nm consist of a broad band (420 nm - 640 nm) characterized by two main contributions peaking at 484 and 533 nm. The overall maximum emission intensity is found for ZnS:3% Ca with internal quantum yield of 8.4%.

Keywords: Hydrothermal synthesis; Ca-doped ZnS nanoparticles; Photoluminescence.

Journal Pre-proof

1. Introduction

The investigation on physico-chemical properties of Nanoparticles (NPs) has gained considerable attention since several years thanks to their potential application in the fabrication of nano-devices. Due to their large surface on volume ratio and quantum confinement effects, the electronic, magnetic and optical properties of NPs get appreciably modified compared to their bulk counterparts [1-4] since the number of active sites occupying the surface area increases with decrease in the particle size.

Mostly, NPs have been prepared from II-VI and from III-V semiconductor groups. These inorganic materials show very important advantages due to their chemical stability and long service life. Among these, zinc sulfide (ZnS) is a typical II–VI semiconductor compound with direct bandgap energy of 3.65 eV and a small Bohr radius [5]. Because of its outstanding luminescence and photochemical properties, ZnS is a potential candidate for solar cells [6], nuclear batteries [7], optoelectronic devices [8], light - emitting diodes (LED) [9] and as sample for bio-sensing and bio-imaging [10-12].

A doping protocol is one of the most intensively utilized means to improve targeted optical, electronic, photocatalytic and textural properties of semiconducting nanomaterials by inserting traps and discrete energy states into the stimulated electrons bandgap. Doping will increase structural defects, modify grain size and increase the contact surface area, which is expected to lead to higher quantum yields for semiconductor materials. Series of ZnS nanocrystals doped with different transition metal (TM) or rare-earth metal (RE) ions have been described in literature. Lin *et al* synthesized ZnS: Cu, ZnS: Ag and ZnS: Au materials using a chemical method [13]; F. Amirian *et al* studied ZnS: TM [14] and D. Kakoti *et al* which reported the optical properties of ZnS: Sm^{3+} [15]. However, only one paper was found in the literature indicating the effect of Ca^{2+} as dopant on the luminescence properties of ZnS nanoparticles [16]. Despite that the authors report an enhancement of the luminescence of ZnS:Ca^{2+} measured on nanoparticles dispersed in methanol under UV excitation at 310 nm, no attention has been paid on the effect and the mechanism of Ca^{2+} ion doping in these ZnS phosphors, notably from the crystallographic point of view, and from the analysis of excitation spectra and kinetics of the luminescence. Same considerations concern recent works on ZnO:Ca NPs where it has been shown that such doping by Ca^{2+} can improve the optical properties of ZnO undoped NPs [17,18]. Hence, Ca^{2+} is a motivational candidate for investigating its effect of luminescence properties.

Several techniques such as chemical vapour deposition, wet chemical route, co-precipitation, solvothermal or hydrothermal processes, thermal decomposition method, radio frequency magnetron sputtering technique and solid state reaction method were used by many researchers to prepare ZnS NPs [19]. Among them the hydrothermal process, which is eco-friendly because of the use of water as a solvent and an inorganic salt as a catalyst for the reaction, appears very suitable due to its ease and high efficiency. Moreover the reagents are non-

toxic and inexpensive. The hydrothermal protocol is widely used as one of the aqueous-phase processes and collected crystals show a strong purity and reasonable dispersion. Besides its benefit stems from higher reliability and the process itself is fast and needs a small thermal supply only. Collection of studies on hydrothermally synthesized ZnS based materials were recently published concerning for instance photo-catalytic or photo-luminescent properties [20,21]. Thus this method was used in the present work for the production of ZnS and Ca-doped ZnS NPs at different concentrations (1.5; 3; 4.5 and 6 mol %).

The choice of Ca^{2+} doping for ZnS NPs is motivated in order to modify the structural properties connected with the zinc environment and see their influence on optical properties. Ca^{2+} ionic radius is higher than that of Zn^{2+}, 1.00 Å (in a 4-fold coordination) [22] versus 0.60 Å (for a 6-fold coordination) [22] and calcium sulphide CaS has rock salt structure with a bandgap energy of 4.8 eV. These differences in physical properties are expected to provide new insights, notably in the target of the production of very efficient Light Emitting Diodes (LEDs) for industrial use.

We report in this paper the undoped and Ca^{2+} doped ZnS NPs synthesis protocol. The impact of Ca^{2+} ions as a dopant factor on structural, textural and optical properties was investigated. The materials characterization was followed using different techniques such as X-Ray diffraction (XRD), Raman scattering spectroscopy, Scanning Electron Microscopy (SEM) and Transmission Electron Microscopy (TEM). In addition, photoluminescence measurements allowed us to carry out a complete study of the influence of Ca^{2+} ions doping.

Journal Pre-proof

2. Experimental

2.1. Materials

Zinc acetate dihydrate ($Zn(CH_3COO)_2$, $2H_2O$), thiourea ($SC(NH_2)_2$) and calcium chloride dihydrate ($CaCl_2$, $2H_2O$) were purchased from Sigma-Aldrich and used without further purification. Deionized water (DI) was used for the synthesis.

2.2. Synthesis of undoped and Ca^{2+} doped ZnS

Undoped and Ca^{2+} doped ZnS NPs were synthesized by a hydrothermal method. In a typical procedure for undoped ZnS materials, 2.94 g (13 mmol) of Zn $(CH_3COO)_2$, $2H_2O$ and 2.44 g (32 mmol) of $SC(NH_2)_2$ powders were dissolved separately in 20 ml of deionized water with continuous stirring. A Zn/S initial molar ratio of 1/2.5, thus corresponding to a sulfur excess compared with the desired formula, was chosen according to the literature [23]. A Zn/S molar ratio of 1/1 corresponding to the desired stoichiometric formula was also tested, but the experimental yield (around 20-25 %) was very low compared to that found with the 1/2.5 molar ratio (about 60%). Then, the solutions were mixed by adding the $SC(NH_2)_2$ solution drop by drop into the $Zn(CH_3COO)_2$, $2H_2O$ solution with vigorous stirring for 30 mn. The final solution was transferred to a 100 ml Teflon-lined stainless steel autoclave which was kept at 180 °C for 20 h. After that the solution was centrifuged and the residue was recovered. The product was washed several times with deionized water and ethanol followed by centrifuging at 4000 rpm for 20 min. The resulting final product was kept for drying in an oven for 12 h at 80 °C to yield ZnS NPs.

The same synthesis protocol including excess of sulfur was used for the Ca^{2+} doped ZnS materials with the nominal formula $Zn_{1-x}Ca_xS$ (with x = 1.5; 3; 4.5; 6 mol %), later named ZnS: x % Ca. For this purpose, the zinc acetate solution was replaced by a Zn/Ca mixed solution

obtained by adding drop by drop a solution of x mmol of $CaCl_2$, $2H_2O$ in 5 mL H_2O in a solution of (1-x) mmol of zinc acetate in 20 mL H_2O with continuous stirring for 10 mn.

2.3. Characterization techniques

2.3.1. Structural and morphological characterizations

The X-ray powder diffraction (XRD) patterns were recorded with a Philips X-Pert Pro diffractometer equipped with an X'Celerator detector and using Cu-K$\alpha_{1,2}$ radiation. Data were collected at room temperature in the range from 10.0° to 75.0° (2θ) with a step width of 0.02° (2θ). All the data were processed by Xpert High Score Plus software using databases (unit cell parameters, peaks identification). Particle size measurements were carried out using Scherrer formula. The surface morphology of the as-prepared NPs was recorded using scanning electron microscopy with a JEOLJSM-7001f device. SEM micrographs were performed using a high vacuum at 20 kV and a back-scatter electron detector. Transmission Electronic Microscopy (TEM) images were recorded on a Hitachi H-7650 microscope at the Centre Imagerie Cellulaire Santé (CICS) of Clermont-Ferrand University.

Polycrystalline samples Raman spectra were recorded at room temperature with a T 64000 JOBIN- YVON spectrometer equipped with a CCD detector cooled with liquid nitrogen. Excitation at 532 nm was supplied with a compact doubled YAG:Nd^{3+} Oxxius laser. The samples were placed under the X50 objective of an Olympus microscope allowing probing a surface of 2 μm^2. A unique measurement cycle was performed for each sample with an acquisition time of 120 s.

Journal Pre-proof

2.3.2. Luminescence analysis

The optical properties were investigated by recording the luminescence spectra with a Horiba-Jobin-Yvon set-up consisting of a Xenon lamp operating at 400 W monochromatized through Triax 180 then the emitted light was dispersed through Triax 550 and detected with the means of a cryogenically cold charge coupled device (CCD) camera (Symphony LN2 series) for emission spectra and Hamamatsu R928 PMT for excitation ones. Temporal evolution of the luminescence were carried out with a pulsed Nd:YAG OPO-Ekspla NT342B laser (3–5 ns pulse duration, 10 Hz, 5 cm^{-1} line width, 210–2600 nm). The emitted photons were detected at right angle from the excitation and analyzed through Edinburgh FLS980 spectrometer (1200 groove mm^{-1} grating, blazed at 500 nm, minimum band-pass of 0.1 nm) equipped with Hamamatsu R928P PMT (200–870 nm).

The internal and external quantum yields (QY) were assessed using a C9920-02G PL-QY measurement system from Hamamatsu. The setup comprises a 150W monochromatized Xe lamp, an integrating sphere (Spectralon® Coating, Ø = 3.3 inch) and a high sensitivity CCD spectrometer for detecting the whole spectral luminescence (the emission spectra were integrated from 400 nm to 650 nm for ZnS and ZnS: Ca compounds). The automatically controlled excitation wavelength range spread from 250 nm to 950 nm (deliberately limited from 300 to 450 nm in this study) with a resolution bandwidth better than 5 nm. Quantum yields excitation spectra were obtained by scanning the excitation and monitoring the overall luminescence. The internal efficiencies correspond to the ratio between the emitted and absorbed photons. All measurements were recorded at room temperature.

3. Results and discussion

3.1. XRD analysis

The X-ray diffraction patterns of undoped and Ca^{2+} (1.5, 3, 4.5 and 6 mol %) doped ZnS NPs are reported in Fig. 1. Whatever the Ca^{2+} content into the ZnS host, these patterns match very well with the JCPDS card 80-0020 corresponding to the cubic blende ZnS structure. No additional diffraction peaks corresponding to the ZnS wurtzite polymorph or secondary phases are present, confirming the validity of the synthesis protocol and that prepared samples are pure in structural form.

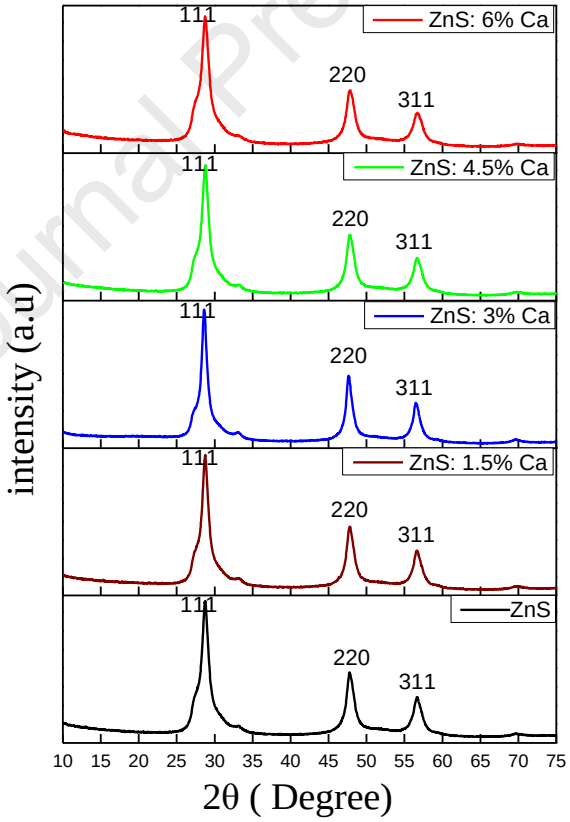

Fig. 1: XRD patterns of ZnS and ZnS: x% Ca NPs.

Journal Pre-proof

Journal Pre-proof

Interestingly there is no significant shifting in the diffraction peaks position. In the ZnS blende structure, the Ca^{2+} ions cannot accommodate the characteristic 4-fold cationic coordination due to their ionic radius significantly higher than that of Zn^{2+} ions [22]. Thus they cannot be incorporated in cubic blende crystallographic sites 4(a). However Ca^{2+} ions can adopt a 6-fold coordination. This feature suggests that Ca^{2+} ions can be incorporated into specific interstitial sites initially vacant in the blende structure (4d sites (x/a=1/4; y/b=3/4; z/c=1/4), see Fig. 2) as demonstrated by D. K. Sen *et al* [24]. Besides, from the ZnS-CaS binary system investigation, no secondary phases are observed taking into account the studied Ca/Zn stoichiometric amounts [25].

Due to these statements, vacancies are created in 4a sites (Zn^{2+} sites) due to Ca^{2+} vicinity, which play a very important role in photoluminescence as will be seen later. Taking into account this crystallographic description a Ca^{2+} cation is surrounded by four first-neighbours Zn^{2+} ions with Ca-Zn distances of about 2.35 Å and six second-neighbours S^{2-} anions with Ca-S distances of about 2.7 Å in agreement with Ca^{2+} environmental description in CaS rock-salt CaS structure [25]. Due to steric hindrance the exclusion of four Zn^{2+} ions present in the first Ca^{2+} coordination shell, three of them located in faces center and the last one located at the top of the cubic cell, leads actually to the disappearance of 1.625 Zn^{2+} ions for one Ca^{2+} ion, due to the fact that Zn^{2+} ions are shared between adjacent cells. These new zinc vacancies are due to the Ca^{2+} doping and are likely to be added to those already existing in the blende framework.

Particle sizes were calculated for each sample using the Scherrer formula [26]:

$$D = \frac{0.9\,\lambda}{\beta\,\cos\theta} \qquad (1)$$

where D is the average particle size, λ is the X-ray wavelength, β is the full width at half maximum (FWHM) and θ is the diffraction angle value. The average particle size calculated, considering all (111), (220) and (311) diffraction planes, slowly increases according to the increase of Ca^{2+} content until a doping value of 3 mol% (see Table 1). Higher doping contents are characterized by a small decrease of the crystallite size. Grain size of nanometric scale was expected taking into account the operating protocol used.

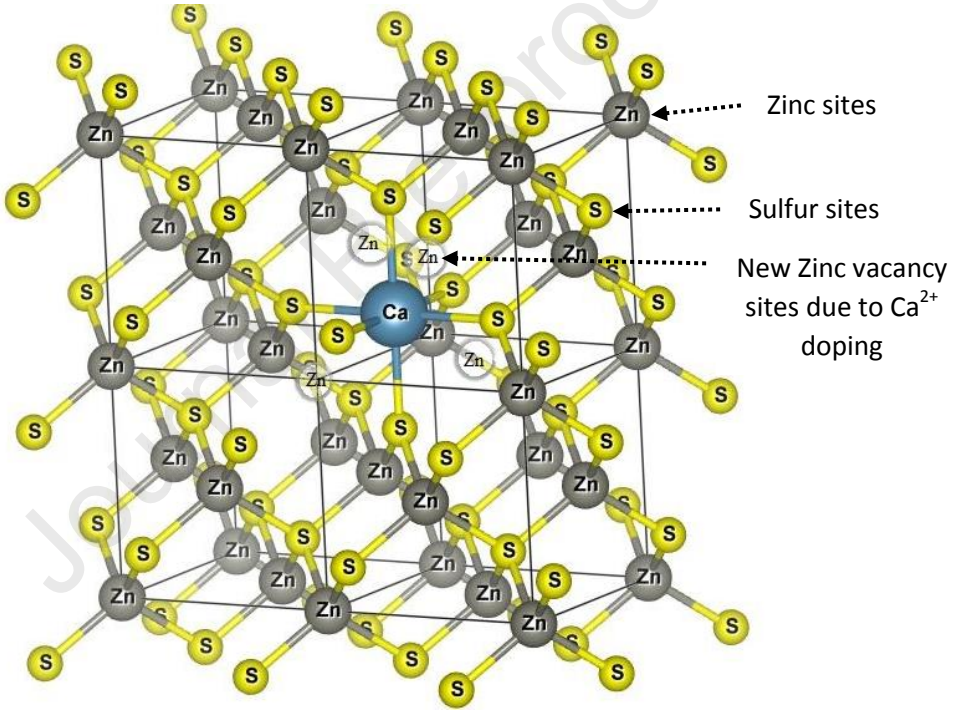

Fig. 2 Crystal structure of ZnS: Ca blende polymorph.

The average lattice constants values were calculated on the basis of the main three (111), (220) and (311) diffraction peaks using the following formula [26]:

$$d_{hkl} = \frac{a}{\sqrt{h^2 + k^2 + l^2}} \qquad (2)$$

Journal Pre-proof

where *h*, *k* and *l* are the Miller indices of the considered Bragg planes. They are gathered in Table 1.

The lattice parameters do not significantly change considering Ca^{2+} doping amounts which provides another proof to the fact that the invited ions are not substituted for Zn^{2+} ones but are located into interstitial sites as shown in Fig. 2.

Table 1 Particle sizes and lattice parameters for ZnS and ZnS: x% Ca NPs.

Sample	Particles size (nm)	Lattice parameter (Å)
ZnS	6.6 (1)	5.379 (2)
ZnS : 1.5% Ca	6.9 (1)	5.380 (2)
ZnS : 3% Ca	8.3 (1)	5.396 (2)
ZnS : 4.5% Ca	6.0 (1)	5.381 (2)
ZnS : 6% Ca	6.2 (1)	5.379 (2)

Journal Pre-proof

3.2. SEM and TEM analysis

SEM images of undoped and Ca^{2+} doped ZnS (x = 6 mol %) are shown in Fig. 3(A). Nanoparticles of undoped and Ca^{2+} doped ZnS materials show a microsphere structure with diameters comprised from 800 nm to 2 μm, which is constructed by nanoparticles self-assembly. These marbles show a smooth surface without any appreciable roughness. All morphologies are similar whatever the doping ion amount in the range 0-6 % Ca.

Fig. 3(B) show the TEM images of undoped and Ca^{2+} doped ZnS NPs (x = 6 mol %). These micrographs confirm the spherical shape of nanoparticles with size distribution comprised in the range 40-140 nm. TEM images corroborate thus that nanoparticles are consistent with isotropically assembled crystallites which mean size was determined by Scherrer law.

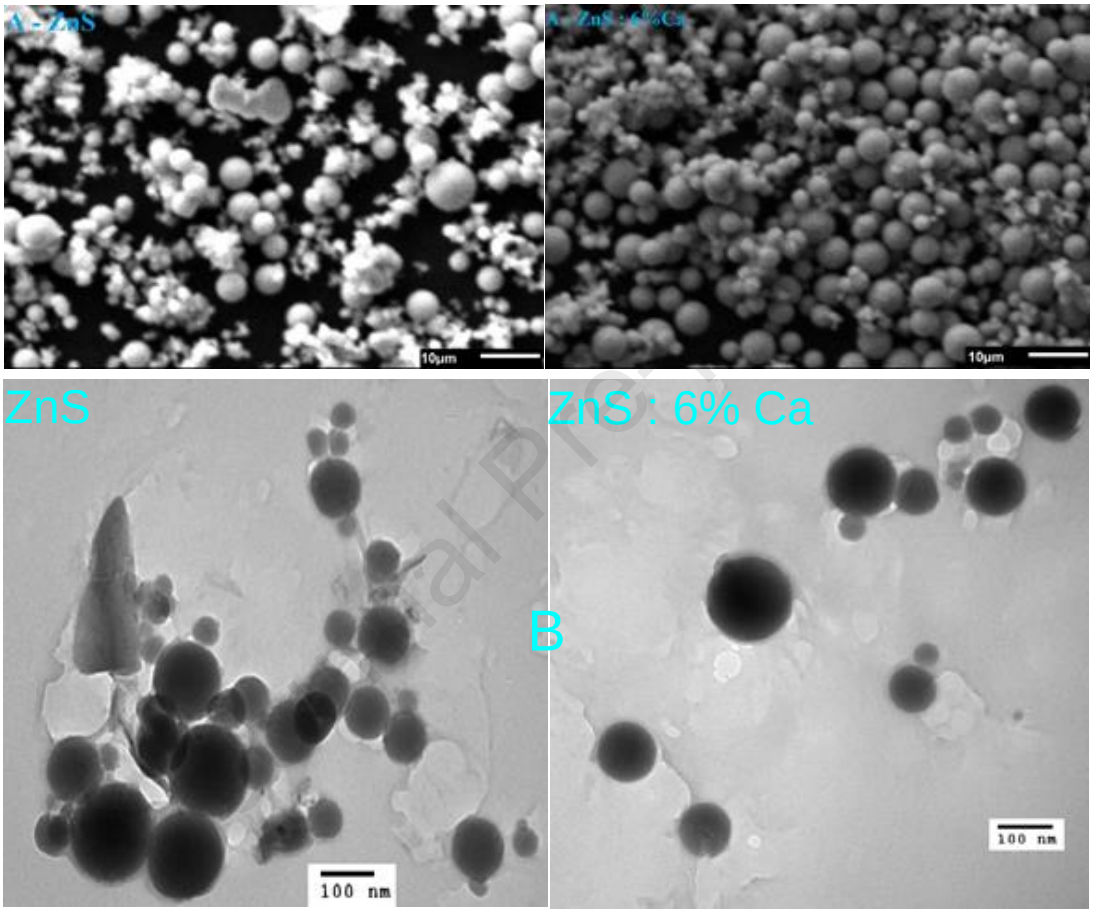

Fig. 3 (A) Scanning electron microscopy (SEM) images of ZnS and ZnS: 6 mol % Ca. (B) Transmission electron microscopy (TEM) images of ZnS and ZnS: 6 mol % Ca.

3.3. Raman scattering

Raman scattering is an inelastic and ~~a~~ non-destructive process to obtain vibrational states information for a solid material. The Raman spectra were recorded at room temperature in order to obtain more detailed structural information of ZnS: Ca x% NPs. Spectra of undoped and Ca^{2+}

doped ZnS samples are reported in Fig. 4. Two characteristic peaks located at 260 and 350 cm^{-1} are well observed. These results are similar to those found by Mou Pal *et al* [27].

The small peak at 260 cm^{-1} can be attributed to the first-order transverse optical mode whereas the relatively intense and broad peak appearing at 350 cm^{-1} is attributed to the first-order longitudinal optical mode of cubic ZnS [28]. No extra bands are observed indicating again the validity of the synthesis protocol.

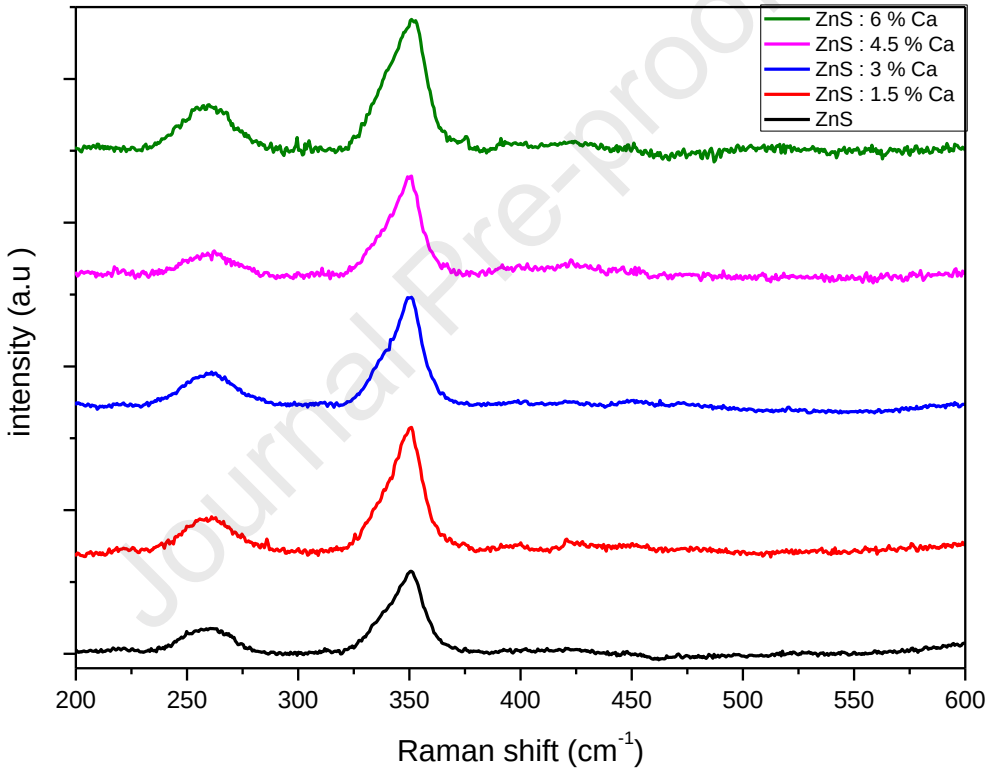

Fig. 4 Raman spectra of ZnS and ZnS: x% Ca NPs.

3.4. Optical properties

The PL-QYs plotted versus the excitation wavelength for undoped and Ca^{2+} doped ZnS are presented in Fig. 5. Overall emission lying between 400 and 650 nm was integrated. The

internal quantum yields obtained at room temperature under a 400 nm (25000 cm^{-1}) excitation are gathered in Table 2.

The excitation PL-QY spectra of all samples show a unique dissymmetric broad band peaking at 25000 cm^{-1} (400 nm) wavelength excitation. The undoped ZnS NPs present an internal QY of 4.7 %, the highest value (8.4%) was obtained for ZnS: 3% Ca, which exhibits the largest crystalline size. Therefore, Ca^{2+} ions doping improves the PL-QYs of ZnS NPs.

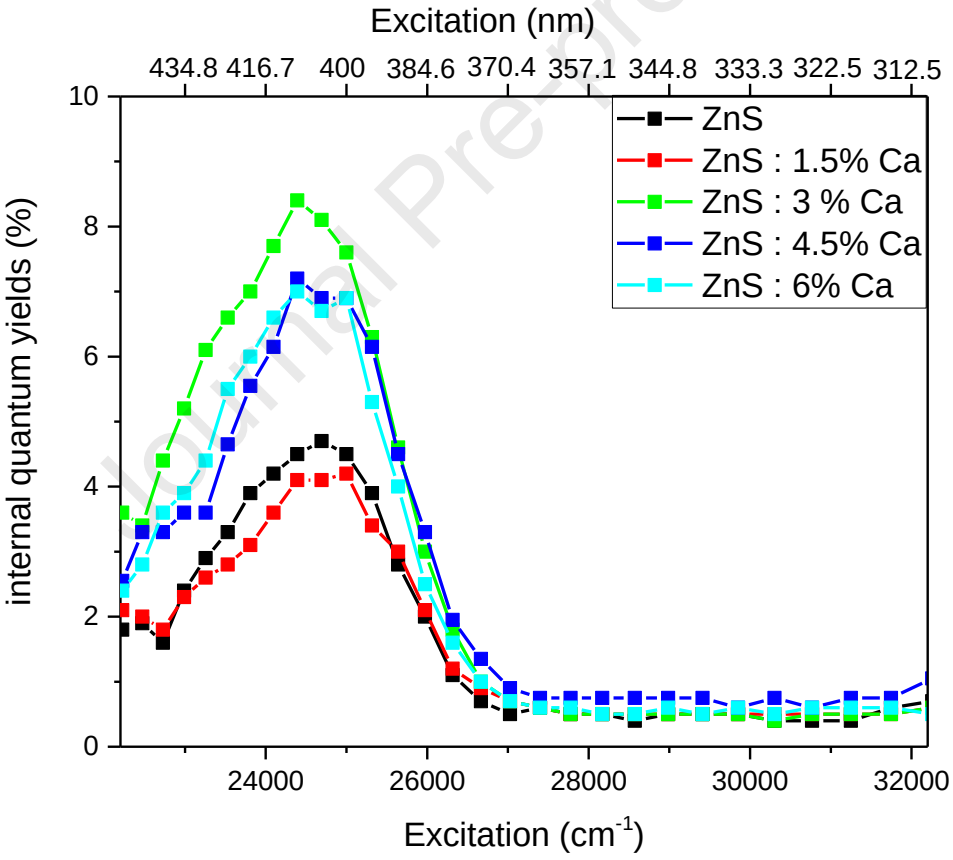

Fig. 5 Internal quantum yield of ZnS and ZnS: x % Ca.

The excitation and emission spectra were recorded at room temperature in the same conditions for all samples. Fig. 6 shows the normalized photoluminescence excitation (PLE) spectra of ZnS: x % Ca phosphors (with x = 0-6 mol %) monitoring an emission wavelength of λ_{em} = 16129 cm^{-1} (620 nm) corresponding to the red emission band edge for avoiding excitation beam scattering. The excitation spectra were recorded from 20000 (500 nm) to 30000 (333 nm) cm^{-1}. All excitation spectra were corrected from the spectral response of the apparatus and are characterized by a unique broad band, centered at 25000 cm^{-1} (400 nm), which corresponds perfectly to the energy gap of this semiconductor. This result is in agreement with the PL-QY reported in Fig. 5. Moreover, no shift due to the Ca^{2+} ions doping is noticed.

Table 2 Internal quantum efficiencies for ZnS and ZnS: x% Ca NPs under 400 nm excitation.

Sample	Internal Quantum Yield (%)
ZnS	4.7
ZnS : 1.5% Ca	4.2
ZnS : 3% Ca	8.4
ZnS : 4.5% Ca	7.2
ZnS : 6% Ca	7.0

The photoluminescence (PL) emission spectra shown in Fig. 7 were recorded from 16000 cm^{-1} to 24000 cm^{-1} under excitation at 25000 cm^{-1} (400 nm) using the OPO laser for all undoped and Ca^{2+} doped samples. A wide emission band centered at 19048 cm^{-1} (525 nm) is observed

whatever the doping ion amounts, the intensity of which varies very little as a function of doping rate.

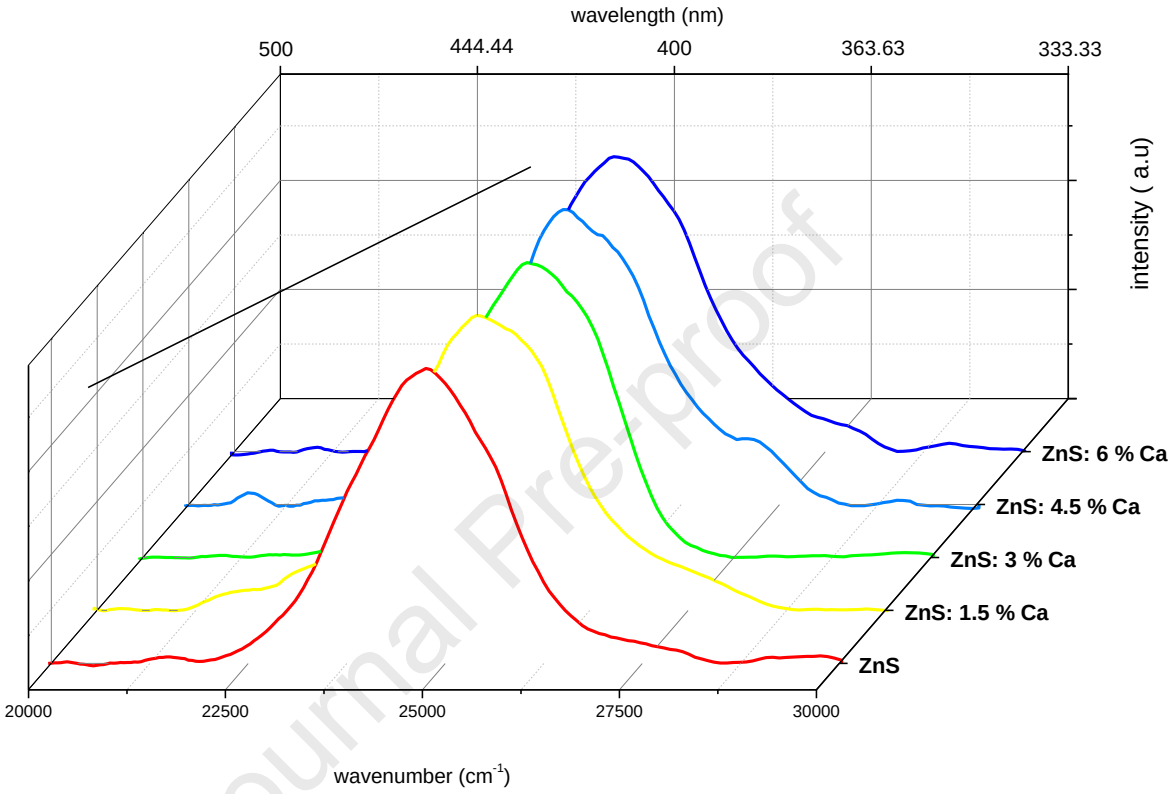

Fig. 6 Photoluminescence excitation spectra ($\lambda_{em} = 16129\ \mathrm{cm}^{-1}$ – 620 nm) of ZnS and ZnS: x% Ca.

Nanocrystals have a very high surface-to-volume ratio due to their very small diameter, which makes them vulnerable to various surface defects. The origin of luminescence was studied by different groups for the undoped ZnS and ZnS doped nanocrystals [2,14,15,27,29-36]. They have demonstrated that the photoluminescence effect is attributed to intrinsic defects due to crystal lattice vacancies such as sulphur and zinc vacancies given that Zn^{2+} and S^{2-} ions are not

luminescent. Besides part of the fluorescence emission is due to introduced dopant ions such as Eu^{3+} [27], Mn^{2+} [29,31,33] or Cu moieties [32].

In our work ZnS and ZnS: Ca show an emission covering the whole visible region. Ca^{2+} is an alkaline-earth ion and thus does not show luminescence properties but its effect as impurity in semiconductor materials would obviously affect emission intensity according to the presented experimental results. The emission band surface area for each sample was calculated for comparison. The results are gathered in Table 3. Thus, the fluorescence efficiencies of ZnS: Ca samples are higher than that of undoped ZnS samples. Ca^{2+} ions doped samples exhibit PL emission intensity approximately twice as high as that of non-doped sample. Besides the fluorescence intensity observed for the different doped samples is almost similar. The calculation of the full-width at half maximum (FWHM) of fluorescence intensity shows that the ZnS: 3% sample has the widest spectral range compared to other samples.

Journal Pre-proof

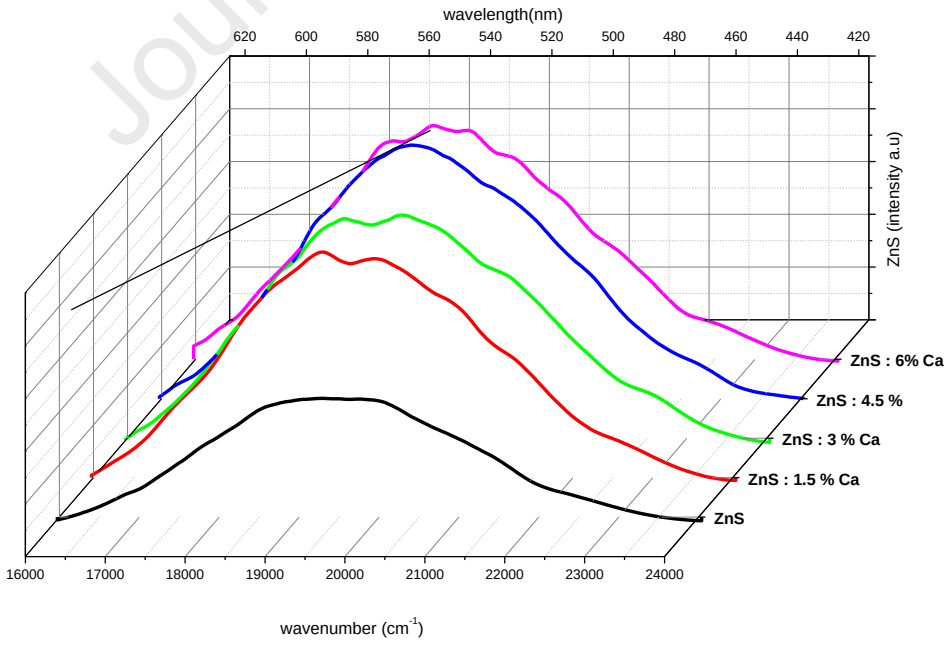

Fig. 7 Photoluminescence emission spectra of ZnS and ZnS: x% Ca NPs (λ_{exc} = 400 nm).

It is observed from Fig. 7 that the emission bands are highly asymmetric and broadened especially at higher wavelength side, indicating that different luminescence centers are involved in radiative processes. A deconvolution of the luminescence band response using a Gaussian law was conducted in order to better understand the emission phenomena. The Gaussian deconvolution of the broad PL emissions for undoped ZnS and 3% Ca^{2+} doped phosphors are presented in Figure 8.

The undoped ZnS emission spectra deconvolution (Fig. 8-A) shows the presence of two bands. The band located at 20660 cm^{-1} (484 nm) is attributed to the emission transition of intrinsic defects due to sulfur vacancies (V_S), whereas the most intense band at around 18762 cm^{-1} (533 nm) is due to the emission transition of intrinsic defects specific to zinc vacancies (V_{Zn}) [23].

Table 3 Area of PL emission spectra.

Sample	Area of photoluminescence emission spectra (a.u.)
ZnS	0.49
ZnS : 1.5% Ca	0.90
ZnS : 3% Ca	0.96
ZnS : 4.5% Ca	1
ZnS : 6 % Ca	0.90

Journal Pre-proof

The intensity of the band corresponding to intrinsic defects linked to V_{Zn} vacancies is higher than that due to intrinsic defects specific of V_S vacancies which is probably due to the fact that the samples synthesis was operated taking into account a 1/2 ratio for Zn/S precursors implying an excessive amount of sulphur. This certainly implies the presence of much more Zn vacancies in the undoped zinc sulfide phosphor than S vacancies. Similar results have been reported by Wei *et al*. [23] who noticed that the difference in intensity between both characteristic transitions varies according to the ratio between the precursor amounts in their hydrothermal protocol.

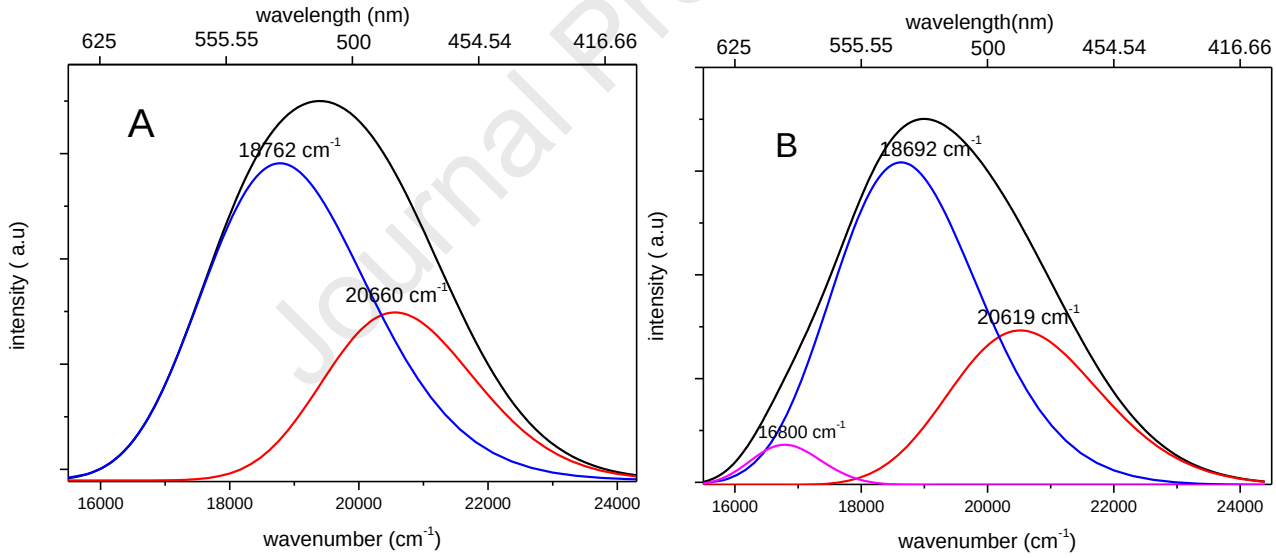

Fig. 8 Gaussian deconvolution of experimental PL emission of (A) undoped ZnS and (B) ZnS: 3 % Ca (λ_{exc} = 400 nm).

The deconvolution of ZnS: 3% Ca (figure 8-B) emission spectrum exhibits the presence of three bands. The first two bands located near 20619 cm^{-1} (485 nm) and 18692 cm^{-1} (535 nm)

are similar to that observed for undoped ZnS samples. A slight shift of wavelengths values is however observed for the 3% Ca doped sample compared to the undoped one. The third band appearing near 16807 cm^{-1} (595 nm) with a very weak intensity is attributed to Ca^{2+} impurity incorporated in 4d sites, which create new energy levels between the valence band and the conduction band as previously reported in the literature [14,17,33]. The Gaussian plot was conducted for all Ca^{2+} doped samples emission bands, the 16807 cm^{-1} (595 nm) band intensity being similar from one sample to another. However, the Ca^{2+} ion contribution is felt on the overall band intensity as shown in Fig. 7.

Although best quantum yields are obtained under excitation at 400 nm (as shown in Fig.5), different emission spectra for the undoped ZnS sample and for the highly doped one (ZnS :6% Ca) were recorded under different excitation wavelenghts as 280, 300, 330 and 360 nm. These PL emission spectra are shown in Fig 9. The emission spectrum recorded under a 400 nm excitation wavelength was reported for comparison. The same features are observed in both figures. A slight red shift is observed depending on the excitation wavelength for a given sample. Moreover a very slight red shift (approximatively 2 nm) is observed for the 6% Ca doped sample for a given excitation wavelength. This was observed in deconvolutions reported in Fig.8. Under excitation at 280 and 300 nm, the emission band is centered near 480 nm and shoulders are recorded near 400 and 430 nm. Under excitation at 330 and 360 nm, the band is shifted towards 500 nm (λ_{exc} = 330 nm) and 505 nm (λ_{exc} = 360 nm). Moreover relatively intense components are recorded near 395, 415 and 440 nm. With λ_{exc} = 400 nm, the main band is observed near 523 nm for undoped ZnS and 525 nm for ZnS : 6% Ca without any visible shoulders.

Journal Pre-proof

These optical features are certainly linked to the presence of impurities originating from raw materials used for NP syntheses especially zinc acetate dihydrate. As evidenced by Saleh *et al* [37] during investigation on undoped commercial ZnS several impurities are detected which are responsible for their own emission band features. Emission bands corresponding to Ag are observed near 400 and 450 nm. Cu impurities give emission bands in the blue region near 420 nm and in the green domain near 520 nm. Band recorded near 470-480 nm correspond to a donor-acceptor pair emission for which isolated Cl^- or Al^{3+} ions act as donors and Zn vacancies-Cl^- (or Al^{3+}) pairs act as acceptors. Saleh *et al* highlighted the following impurities amount: 0.39 ppm for Cu, about 0.03 ppm for Ag and 1.5 ppm for Al. As evidenced by Sigma-Aldrich data sheet analysis for zinc acetate dihydrate, amounts of chlorine contaminant is about 5 ppm. No evidence of Cu, Ag and Al is given in the analysis sheet probably due to their very low amount. However presence of copper is not excluded due to similar atomic mass. Cu contaminant probably comes from the Zn source. Other elements such as iron and lead are analysed as contaminants (5 ppm for Fe and 20 ppm for Pb). However it is difficult to detect Pb impurities in our samples since ZnS:Pb phosphors are characterized by a broad band centered near 580 nm under a 363 nm excitation [38]. The role of contaminants in our samples needs more precise investigations. This will be carried out in further works.

Journal Pre-proof

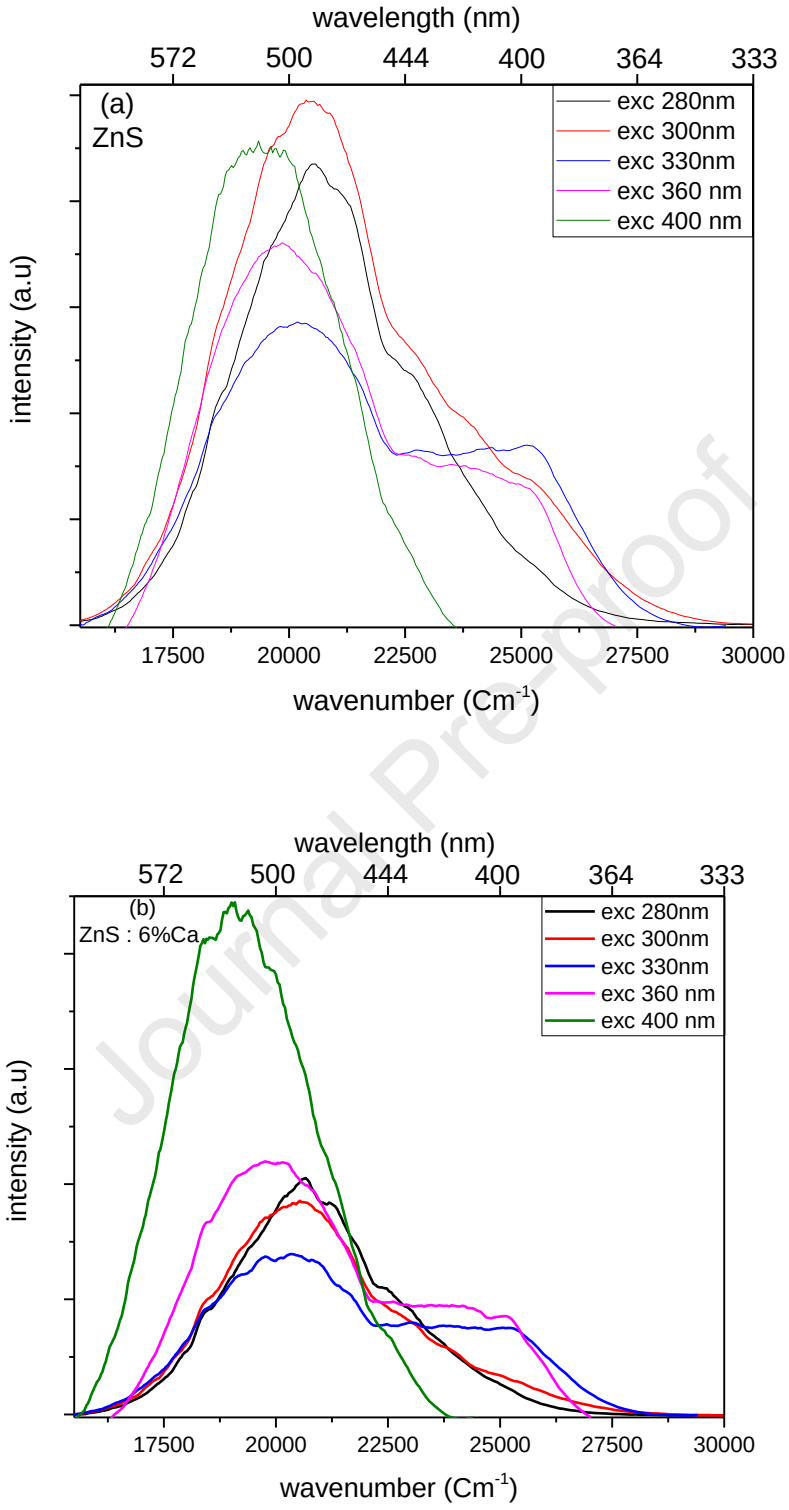

Fig. 9 Photoluminescence emission spectra of undoped ZnS (a) and ZnS: 6 % Ca (b) NPs under different excitation wavelengths.

The decay curves recorded for each ZnS: x% Ca sample (x = 0; 1.5; 3; 4.5 and 6) under excitation at 25000 cm^{-1} (400 nm), monitoring the emission at its maximum located at 19048 cm^{-1} (525 nm) are reported in Fig. 10.

As observed in Fig. 10 all the decays diverge from single exponential shape. In order to estimate the PL decay times, the photoluminescence decay curves were fitted assuming a bi-exponential law given by the following equation [39]:

$$I(t) = C + A_1 e^{-t/\tau_1} + A_2 e^{-t/\tau_2} \quad (3)$$

where A_1 and A_2 are the amplitudes of each decay component, τ_1 and τ_2 are the decay times. I(t) is the luminescence intensity at time t and C a constant. The calculated results are gathered in Table 4.

As observed from the Gaussian deconvolution (see Fig. 8), the emission band covers two main components due to zinc and sulphur vacancies, with respective emissions peaking at 18692 cm^{-1} (535 nm) and 20619 cm^{-1} (485 nm) wavenumbers (wavelengths). According to Wei *et al* [23] a lifetime value increase is correlated to an increase of the intrinsic defects amount. Taking into account the synthesis protocol intrinsic defects due to Zn vacancies are supposed to be prominent, thus τ_2 time constant values corresponding to the band located at 18692 cm^{-1} (535 nm) are higher than τ_1 lifetime values corresponding to the band located at 20619 cm^{-1} (485 nm). As discussed in the crystallographic section (3.1) a Ca^{2+} doping results in an increase of intrinsic defects linked to Zn vacancies. Therefore this implies an increase of τ_2 lifetime values for Ca^{2+} doped materials in comparison with undoped one. However τ_1 lifetime values are weakly influenced by the Ca doping due to the synthesis protocol. τ_1 and τ_2 lifetime values are independent of Ca^{2+} doping amounts. Such observation can be connected to a lack of structural

defects other than those related to zinc and sulphur vacancies or chemical impurities. Attempts of PL decay curves fitting with a tri-exponential formula taking into account the third emission band due to Ca^{2+} impurities do not lead to operable results which is probably due to the very weak intensity of the corresponding emission band located near 16807 cm^{-1} (595 nm).

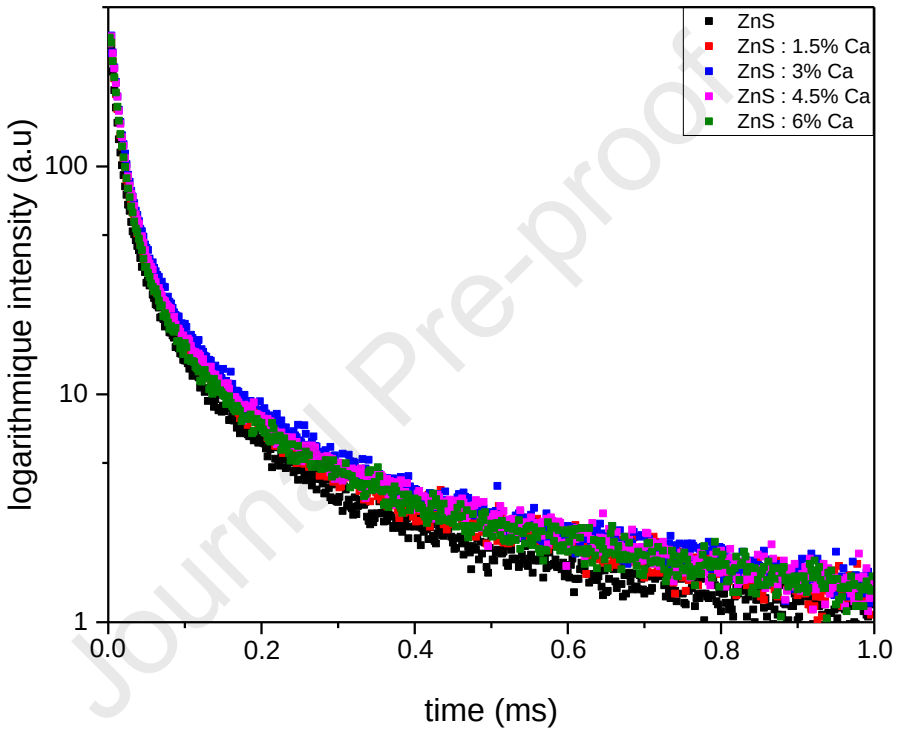

Fig. 10 Photoluminescence decay curves recorded for ZnS and ZnS: x% Ca NPs samples at 19048 cm^{-1} under excitation at 25000 cm^{-1} (400 nm).

Journal Pre-proof

Table 4 Lifetime values for ZnS and ZnS: x% Ca NPs (λ_{exc} = 400 nm).

Sample	τ_1 (µs)	A_1 (a.u)	τ_2 (µs)	A_2 (a.u)
ZnS	11.4	387	83.4	43
ZnS : 1.5% Ca	12.7	576	90.7	43
ZnS : 3% Ca	14.4	374	105.8	45
ZnS : 4.5% Ca	15.3	352	105.4	40
ZnS : 6% Ca	14.6	341	108.1	34

Moreover decay curves were recorded for each excitation wavelength (λ_{exc} = 280, 300, 330, 360 nm, see Fig.9) monitoring the main band emission. These experimental decays are well fitted by a bi-exponential law. A_1-A_2 amplitude and τ_1-τ_2 decay time values are gathered in Table 5. Typical values calculated under a 400 nm excitation wavelength are indicated for comparison. For excitation wavelengths lower than 400 nm, τ_1 and τ_2 lifetime values are slightly higher than values calculated for the 400 nm excitation and are not influenced by the excitation wavelength value. The longer τ_1 and τ_2 lifetime values are probably due to the influence of optically active impurities whose characteristic emission features are superimposed with that of ZnS undoped and doped samples.

ZnS				
λ_{exc} (nm)	τ_1 (µs)	A_1 (a.u)	τ_2 (µs)	A_2 (a.u)
280	22.7	10829	110 .4	811
300	25.1	8718	113.5	1527
330	20.1	6358	105.8	565
360	23.6	7994	131.9	535
400	11.4	387	83.4	43

ZnS : 6% Ca				
λ_{exc} (nm)	τ_1 (µs)	A_1 (a.u)	τ_2 (µs)	A_2 (a.u)
280	23.0	11247	113.7	977
300	22.6	8730	107.6	1024
330	21.0	6457	110.4	501
360	23.9	9659	130.0	700
400	14.6	341	108.1	34

Table 5 Lifetime values for ZnS and ZnS: 6% Ca NPs under different excitation wavelengths.

4. Conclusion

A simple hydrothermal method was carried out to synthesize undoped and Ca^{2+} doped ZnS NPs with a maximal doping amount of 6 mol %. The physico-chemical, morphological and optical properties were investigated using XRD, SEM, TEM, Raman spectroscopy and luminescence technique. All samples exhibit a zinc sulfide blende-type structure as confirmed by X-Ray diffraction and Raman scattering, with particle sizes included in the range 6.0-8.3 nm, and

demonstrated that Ca^{2+} ions are incorporated into the vacant sites leading to additional zinc deficiencies. Furthermore, the SEM/TEM analyses show that NPs present a micro-spherical structure.

PL excitation spectra show a characteristic band centered at 400 nm with no meaningful shifting from undoped to doped samples. PL emission spectra show a highly asymmetric and broadened emission band covering the whole visible region, with multiple contributions indicating the involvement of different luminescence centers in the radiative process. A Gaussian deconvolution shows the presence of two main bands for the non-doped sample due to intrinsic defects related to sulfur vacancies (V_S) located at 20619 cm^{-1} (484 nm) and zinc vacancies (V_{Zn}) at 18692 cm^{-1} (535 nm). In addition a third small band located at 16800 cm^{-1} (595 nm) is observed for all doped samples and is attributed to the effect of the Ca^{2+} impurity. The best quantum efficiency for all samples is reached under 25000 cm^{-1} (400 nm) wavenumber (wavelength) excitation. Lifetime measurements have confirmed the presence of two main transitions due to zinc and sulphur vacancies (V_{Zn}, V_S). Variation of the excitation wavelength shows clearly that some contributions in the emission spectra can arise from the existence of impurities lying in the raw materials used in the synthesis process.

Journal Pre-proof

Acknowledgements

A.S. Messalti gratefully acknowledges the Algerian Ministry of Higher Education and Scientific Research (MESRS), the General Directorate of Scientific Research and Technological Development (DGRSDT) as well as the Ferhat Abbas Sétif 1 University for financial support.

References:

[1] C.X. Liu, Y.Y. Ji, T.W. Tan, One-pot hydrothermal synthesis of water-dispersible ZnS quantum dots modified with mercaptoacetic acid, J. Alloys Compd. 570 (2013) 23–27.

[2] N.S. Nirmala Jothi, A.G. Joshi, R. Jerald Vijay, A. Muthuvinayagam, P. Sagayaraj, Investigation on one-pot hydrothermal synthesis, structural and optical properties of ZnS quantum dots, Mater. Chem. Phys. 138 (2013) 186–191.

[3] B. Poornaprakash, P.T. Poojitha, U. Chalapathi, S.H. Park, Achieving room temperature ferromagnetism in ZnS nanoparticles via Eu^{3+} doping, Mater. Lett. 181 (2016) 227–230.

[4] S.M. El-Bashir, Coumarin-doped PC/CdSSe/ZnS nanocomposite films: A reduced self-absorption effect for luminescent solar concentrators, J. Lumin. 206 (2019) 426–431.

[5] Y.C. Zhang, G.Y. Wang, X.Y. Hu, W.W. Chen, Solvothermal synthesis of uniform hexagonal-phase ZnS nanorods using a single-source molecular precursor, Mater. Res. Bull. 41 (2006) 1817–1824.

[6] Y. Wang, J. Li, J.S. Li, C.H. Duan, H.N. Zhang, H.M. Jian, L. He, G.H. Tao, C. Yan, T.G. Jiu, Solution prepared O-doped ZnS nanocrystals: Structure characterization, energy level engineering and interfacial applications in polymer solar cells, Sol. Energy 160 (2018) 353–359.

[7] Z.H. Xu, X.B. Tang, L. Hong, Y.P. Liu, D. Chen, Structural effects of ZnS: Cu phosphor layers on beta radio luminescence nuclear battery, J. Radioanal. Nucl. Chem. 303 (2015) 2313-2320.

[8] W.S. Ni, Y.J. Lin, Conduction behavior conversion for Cu-doped ZnS/n-type Si devices with different Cu contents, Appl. Phys. A 119 (2015) 1127–1132.

[9] S. Gupta, J.C. McClure, V.P. Singh, Phosphor efficiency and deposition temperature in ZnS: Mn A.C. thin film electroluminescence display devices, Thin Solid Films 299 (1997) 33–37.

Journal Pre-proof

[10] M. Geszke, M. Murias, L. Balan, G. Medjahdi, J. Korczynski, M. Moritz, J. Lulek, R. Schneider, Folic acid-conjugated core/shell ZnS:Mn/ZnS quantum dots as targeted probes for two photon fluorescence imaging of cancer cells, Acta Biomater. **7** (2011) 1327–1338.

[11] R. Ban, J.J. Li, J.T. Cao, P.H. Zhang, J.R. Zhang, J.J. Zhu, Highly luminescent glutathione-capped ZnS: Mn/ZnS core/shell doped quantum dots for targeted mannosyl groups expression on the cell surface, Anal. Meth. 5 (2013) 5929-5937.

[12] M. Sajimol Augustine, A. Anas, A.V. Das, S. Sreekanth, S. Jayalekshmi, Cytotoxicity and cellular uptake of ZnS: Mn nanocrystals biofunctionalized with chitosan and amino acids, Spectrochim. Acta. A. Mol. Biomol. Spectrosc. 136 (2015) 327–333.

[13] K.B. Lin, Y.H. Su, Photoluminescence of Cu: ZnS, Ag: ZnS, and Au: ZnS nanoparticles applied in Bio-LED. Appl. Phys. B 113 (2013) 351–359.

[14] F. Amirian, M. Molaei, M., M. Karimipour, A.R. Bahador, A new and simple UV-assisted approach for synthesis of water soluble ZnS and transition metals doped ZnS nanoparticles (NPs) and investigating optical and photocatalyst properties, J. Lumin. 196 (2018) 174–180.

[15] D. Kakoti, P. Dutta, P. Gogoi, N. Dehingia, N. Rajkonwar, A. Boruah, A.T.T Mostako, P.K. Saikia, P.K. Gogoi, Corrigendum to: "Effect of ZnS nanoparticles on the Judd-Ofelt and radiating parameters of Sm^{3+} ions in sol-gel silica Matrix" , J. Lumin. 213 (2019) 451–453.

[16] C.S. Pathak, M. K. Mandal, Structural and optical properties of Ca^{2+} doped ZnS nanoparticles, Nanosci. Nanotechnol., Lett. 6(8) (2014) 681-684.

[17] L. El Mir, Luminescence properties of calcium doped zinc oxide nanoparticles Journal of Luminescence 186 (2017) 98–102.

[18] P. Visali, R. Bhuvaneswari, Photoluminescence and enhanced photocatalytic activity of ZnO nanoparticles through incorporation of metal dopants Al and Ca. Optik 202 (2020) 163706.

Journal Pre-proof

[19] S. Suganya, M. Jothibas, S.J. Jeyakumar, Solid state synthesis of cadmium doped ZnS with excellent photocatalytic activity and enhanced visible light emission. J. Mater. Sci. Mater. Electron. 30 (2019) 7916–7927.

[20] S. Kakarndee, S. Juabrum, S. Nanan, Low temperature synthesis, characterization and photoluminescence study of plate-like ZnS, Mater. Lett. 164 (2016) 198–201.

[21] Q. Ma, Y.Q. Wang, J.H. Kong, H.X. Jia, Tunable synthesis, characterization and photocatalytic properties of various ZnS nanostructures, Ceram. Int. 42 (2016) 2854–2860.

[22] R.D. Shannon, C.T. Prewitt, Effective ionic radii in oxides and fluorides, Acta Crystallogr. B 25 (1969) 925–946.

[23] Z. Wei, Y. Lu, J. Zhao, S. Zhao, R. Wang, N. Fu, X. Li, L. Guan, F. Teng, Synthesis and Luminescent Modulation of ZnS Crystallite by a Hydrothermal Method, ACS Omega 3 (2018) 137–143.

[24] D. K. Sen, S. Bhusha, Structural Studies of Some Zinc and Calcium Sulfide Phosphors Cryst. Res. Technol. 30(7) (1995) 943-947

[25] J. Gao, Y. Duan, C.M. Zhao, W. Liu, H. Dong, D. Zhang, H. Dong, Prediction of new ZnS–CaS alloys with anomalous electronic properties. J. Mater. Chem. C**7** (2019) 1246–1254.

[26] L.S. Birks, H. Friedman, Particle Size Determination from X- Ray Line Broadening, J. Appl. Phys. 17 (1946) 687–692.

[27] M. Pal, N.R. Mathews, E.R. Morales, J.M. Gracia y Jiménez, X. Mathew, Synthesis of Eu^{+3} doped ZnS nanoparticles by a wet chemical route and its characterization. Opt. Mater. 35 (2013) 2664–2669.

[28] S. Dhara, A.K. Arora, S. Bera, J. Ghatak, Multiphonon probe in ZnS quantum dots, J. Raman Spectrosc. 41 (2010) 1102–1105.

Journal Pre-proof

[29] R. Sarkar, C.S. Tiwary, P. Kumbhakar, S. Basu, A.K. Mitra, Yellow-orange light emission from Mn^{2+}-doped ZnS nanoparticles, Physica E Low-Dimens. Syst. Nanostructures 40 (2008) 3115–3120.

[30] S. Sapra, A. Prakash, A. Ghangrekar, N. Periasamy, D.D. Sarma, Emission Properties of Manganese-Doped ZnS Nanocrystals, J. Phys. Chem. B 109 (2005) 1663–1668.

[31] W. Chen, V.F. Aguekian, N. Vassiliev, A.Y. Serov, N.G. Filosofov, New observations on the luminescence decay lifetime of Mn^{2+} in ZnS: Mn^{2+} nanoparticles, J. Chem. Phys. 123 (2005) 124707.

[32] B. Belache, Y. Khelfaoui, M. Bououdina, T. Souier, W. Cai, Photoluminescence of ZnS:Cu quantum dots embedded in silica thin films. J. Lumin. 207 (2019) 258–265.

[33] L. Hu, Y., Hu, B., Yang, D. & Wei, Z. Suppression of blue photoluminescence and enhancement of green photoluminescence by Mn and Cu Co-doped ZnS quantum dots. J. Mater. Sci. Mater. Electron. 31 (2020) 2617–2624.

[34] T.P. Nguyen, Q.V. Lam, T.B. Vu, Effects of precursor molar ratio and annealing temperature on structure and photoluminescence characteristics of Mn-doped ZnS quantum dots. J. Lumin. 196 (2018) 359–367.

[35] S.J. Basha, V. Khidhirbrahmendra, J. Madhavi, U.S. Udayachandran Thampy, C.V. Reddy, R.V.S.S.N. Ravikumar, Structural, optical, magnetic and thermal investigations on Cr^{3+} ions doped ZnS nanocrystals by co-precipitation method. J. Sci. Adv. Mater. Devices 4 (2019) 260-266.

[36] K.C. Kumar, N.M. Rao, S. Kaleemulla, G.V. Rao, Structural, optical and magnetic properties of Sn doped ZnS nano powders prepared by solid state reaction. Physica B Condens. Matter 522 (2017) 75–80.

Journal Pre-proof

[37] M. Saleh, K.G. Lynn, L.G. Jacobsohn, J.S. McCloy, Luminescence of undoped commercial ZnS crystals: A critical review and new evidence on the role of impurities using photoluminescence and electrical transient spectroscopy, J. Appl. Phys. 125 (2019) 075702.

[38] P. Yang, M. Lu, D. Xu, D. Yuan, G. Zhou, Photoluminescence properties of ZnS nanoparticles co-doped with Pb^{2+} and Cu^{2+}, Chem. Phys. Lett. 336 (2001) 76-80.

[39] U. Woggon, Optical properties of semiconductor quantum dots, Vol. 136, Springer Ed. (1996).

Journal Pre-proof

Highligths

- Ca^{2+} doped ZnS NPs were synthesis by a facile hydrothermal method.
- PL excitation spectra show a characteristic band centered at 400 nm.
- PL emission spectra show a large emission band covering the whole visible region.
- Deconvolution of luminescence spectra shows the presence of two main bands for the non-doped sample due to intrinsic defects related to V_S and V_{Zn}.
- The Ca^{2+} doped materials show higher luminescence intensity, greater quantum yield and longer lifetime than undoped material.

Journal Pre-proof

Journal Pre-proof

Declaration of interests

☒ The authors declare that they have no known competing financial interests or personal relationships that could have appeared to influence the work reported in this paper.

☐The authors declare the following financial interests/personal relationships which may be considered as potential competing interests:

Journal Pre-proof